

Euclid Quick Data Release (Q1)

The strong-lensing discovery engine d: Double-source-plane lens candidates

Euclid Collaboration: T. Li¹, T. E. Collett¹, M. Walmsley^{2,3}, N. E. P. Lines¹, K. Rojas^{4,1}, J. W. Nightingale⁵, W. J. R. Enzi¹, L. A. Moustakas⁶, C. Krawczyk¹, R. Gavazzi^{7,8}, G. Despali^{9,10,11}, P. Holloway¹², S. Schuldt^{13,14}, F. Courbin^{15,16}, R. B. Metcalf^{9,10}, D. J. Ballard^{1,17}, A. Verma¹², B. Clément^{18,19}, H. Degaudenzi²⁰, A. Melo^{21,22}, J. A. Acevedo Barroso¹⁸, L. Leuzzi^{9,10}, A. Manjón-García²³, R. Pearce-Casey²⁴, D. Sluse²⁵, C. Tortora²⁶, R. Massey²⁷, G. Mahler^{25,28,27}, A. More^{29,30}, N. Aghanim³¹, B. Altieri³², A. Amara³³, S. Andreon³⁴, N. Auricchio¹⁰, H. Aussel³⁵, C. Baccigalupi^{36,37,38,39}, M. Baldi^{40,10,11}, A. Balestra⁴¹, S. Bardelli¹⁰, P. Battaglia¹⁰, R. Bender^{42,43}, F. Bernardeau^{44,8}, A. Biviano^{37,36}, A. Bonchi⁴⁵, E. Branchini^{46,47,34}, M. Brescia^{48,26}, J. Brinchmann^{49,50}, S. Camera^{51,52,53}, G. Cañas-Herrera^{54,55,56}, V. Capobianco⁵³, C. Carbone¹⁴, V. F. Cardone^{57,58}, J. Carretero^{59,60}, S. Casas⁶¹, M. Castellano⁵⁷, G. Castignani¹⁰, S. Cavuoti^{26,62}, K. C. Chambers⁶³, A. Cimatti⁶⁴, C. Colodro-Conde⁶⁵, G. Congedo⁶⁶, C. J. Conselice³, L. Conversi^{67,32}, Y. Copin⁶⁸, H. M. Courtois⁶⁹, M. Cropper⁷⁰, A. Da Silva^{71,72}, G. De Lucia³⁷, A. M. Di Giorgio⁷³, C. Dolding⁷⁰, H. Dole³¹, F. Dubath²⁰, C. A. J. Duncan³, X. Dupac³², S. Escoffier⁷⁴, M. Fabricius^{42,43}, M. Farina⁷³, R. Farinelli¹⁰, F. Faustini^{45,57}, S. Ferriol⁶⁸, F. Finelli^{10,75}, S. Fotopoulou⁷⁶, M. Frailis³⁷, E. Franceschi¹⁰, S. Galeotta³⁷, K. George⁴³, W. Gillard⁷⁴, B. Gillis⁶⁶, C. Giocoli^{10,11}, P. Gómez-Alvarez^{77,32}, J. Gracia-Carpio⁴², B. R. Granett³⁴, A. Grazian⁴¹, F. Grupp^{42,43}, S. V. H. Haugan⁷⁸, H. Hoekstra⁵⁶, W. Holmes⁶, I. M. Hook⁷⁹, F. Hormuth⁸⁰, A. Hornstrup^{81,82}, P. Hudelot⁸, K. Jahnke⁸³, M. Jhabvala⁸⁴, B. Joachimi⁸⁵, E. Keihänen⁸⁶, S. Kermiche⁷⁴, A. Kiessling⁶, B. Kubik⁶⁸, M. Kümmel⁴³, M. Kunz⁸⁷, H. Kurki-Suonio^{88,89}, Q. Le Boulc'h⁹⁰, A. M. C. Le Brun⁹¹, D. Le Mignant⁷, S. Ligori⁵³, P. B. Lilje⁷⁸, V. Lindholm^{88,89}, I. Lloro⁹², G. Mainetti⁹⁰, D. Maino^{13,14,93}, E. Maiorano¹⁰, O. Mansutti³⁷, S. Marcin⁹⁴, O. Marggraf⁹⁵, M. Martinelli^{57,58}, N. Martinet⁷, F. Marulli^{9,10,11}, S. Maurogordato⁹⁶, E. Medinaceli¹⁰, S. Mei^{97,98}, Y. Mellier^{99,8}, M. Meneghetti^{10,11}, E. Merlin⁵⁷, G. Meylan¹⁸, A. Mora¹⁰⁰, M. Moresco^{9,10}, L. Moscardini^{9,10,11}, R. Nakajima⁹⁵, C. Neisser^{101,60}, R. C. Nichol³³, S.-M. Niemi⁵⁴, C. Padilla¹⁰¹, S. Paltani²⁰, F. Pasian³⁷, K. Pedersen¹⁰², W. J. Percival^{103,104,105}, V. Pettorino⁵⁴, S. Pires³⁵, G. Polenta⁴⁵, M. Poncet¹⁰⁶, L. A. Popa¹⁰⁷, L. Pozzetti¹⁰, F. Raison⁴², R. Rebolo^{65,108,109}, A. Renzi^{110,111}, J. Rhodes⁶, G. Riccio²⁶, E. Romelli³⁷, M. Roncarelli¹⁰, R. Saglia^{43,42}, Z. Sakr^{112,113,114}, D. Sapone¹¹⁵, B. Sartoris^{43,37}, J. A. Schewtschenko⁶⁶, M. Schirmer⁸³, P. Schneider⁹⁵, T. Schrabback¹¹⁶, A. Secroun⁷⁴, G. Seidel⁸³, M. Seiffert⁶, S. Serrano^{117,118,119}, P. Simon⁹⁵, C. Sirignano^{110,111}, G. Sirri¹¹, A. Spurio Mancini¹²⁰, L. Stanco¹¹¹, J. Steinwagner⁴², P. Tallada-Crespí^{59,60}, A. N. Taylor⁶⁶, I. Tereno^{71,121}, N. Tessore⁸⁵, S. Toft^{122,123}, R. Toledo-Moreo¹²⁴, F. Torradeflot^{60,59}, I. Tutusaus¹¹³, E. A. Valentijn¹²⁵, L. Valenziano^{10,75}, J. Valiviita^{88,89}, T. Vassallo^{43,37}, G. Verdoes Kleijn¹²⁵, A. Veropalumbo^{34,47,46}, Y. Wang¹²⁶, J. Weller^{43,42}, A. Zacchei^{37,36}, G. Zamorani¹⁰, F. M. Zerbi³⁴, E. Zucca¹⁰, V. Allevalo²⁶, M. Ballardini^{127,128,10}, M. Bolzonella¹⁰, E. Bozzo²⁰, C. Burigana^{129,75}, R. Cabanac¹¹³, A. Cappi^{10,96}, D. Di Ferdinando¹¹, J. A. Escartin Vigo⁴², L. Gabarra¹², M. Huertas-Company^{65,130,131,132}, J. Martín-Fleitas¹⁰⁰, S. Matthew⁶⁶, N. Mauri^{64,11}, A. Pezzotta^{133,42}, M. Pöntinen⁸⁸, C. Porciani⁹⁵, I. Risso¹³⁴, V. Scottez^{99,135}, M. Sereno^{10,11}, M. Tenti¹¹, M. Viel^{36,37,39,38,136}, M. Wiesmann⁷⁸, Y. Akrami^{137,138}, S. Alvi¹²⁷, I. T. Andika^{22,21}, S. Anselmi^{111,110,139}, M. Archidiacono^{13,93}, F. Atrio-Barandela¹⁴⁰, K. Benson⁷⁰, P. Bergamini^{13,10}, D. Bertacca^{110,41,111}, M. Bethermin¹⁴¹, A. Blanchard¹¹³, L. Blot^{142,139}, M. L. Brown³, S. Bruton¹⁴³, A. Calabro⁵⁷, F. Caro⁵⁷, C. S. Carvalho¹²¹, T. Castro^{37,38,36,136}, F. Cogato^{9,10}, A. R. Cooray¹⁴⁴, O. Cucciati¹⁰, S. Davini⁴⁷, F. De Paolis^{145,146,147}, G. Desprez¹²⁵, A. Díaz-Sánchez²³, J. J. Diaz¹³⁰, S. Di Domizio^{46,47}, J. M. Diego¹⁴⁸, P.-A. Duc¹⁴¹, A. Enia^{40,10}, Y. Fang⁴³, A. G. Ferrari¹¹, P. G. Ferreira¹², A. Finoguenov⁸⁸, A. Fontana⁵⁷, A. Franco^{146,145,147}, K. Ganga⁹⁷, J. García-Bellido¹³⁷, T. Gasparetto³⁷, V. Gautard¹⁴⁹, E. Gaztanaga^{119,117,1}, F. Giacomini¹¹, F. Gianotti¹⁰, G. Gozaliasl^{150,88}, M. Guidi^{40,10}, C. M. Gutierrez¹⁵¹, A. Hall⁶⁶, W. G. Hartley²⁰, C. Hernández-Monteagudo^{109,65}, H. Hildebrandt¹⁵², J. Hjorth¹⁰², M. Jauzac^{28,27,153,154}, J. J. E. Kajava^{155,156}, Y. Kang²⁰, V. Kansal^{157,158}, D. Karagiannis^{127,159}, K. Kiiveri⁸⁶, C. C. Kirkpatrick⁸⁶, S. Kruk³², J. Le Graet⁷⁴, L. Legrand^{160,161}, M. Lembo^{127,128}, F. Lepori¹⁶², G. Leroy^{28,27}, G. F. Lesci^{9,10}

J. Lesgourgues⁶¹, T. I. Liaudat¹⁶³, A. Loureiro^{164, 165}, J. Macias-Perez¹⁶⁶, G. Maggio³⁷, M. Magliocchetti⁷³, F. Mannucci¹⁶⁷, R. Maoli^{168, 57}, C. J. A. P. Martins^{169, 49}, L. Maurin³¹, M. Migliaccio^{170, 171}, M. Miluzio^{32, 172}, P. Monaco^{173, 37, 38, 36}, C. Moretti^{39, 136, 37, 36, 38}, G. Morgante¹⁰, S. Nadathur¹, K. Naidoo¹, A. Navarro-Alsina⁹⁵, S. Nesseris¹³⁷, F. Passalacqua^{110, 111}, K. Paterson⁸³, L. Patrizii¹¹, A. Pisani^{74, 174}, D. Potter¹⁶², S. Quai^{9, 10}, M. Radovich⁴¹, P.-F. Rocci³¹, S. Sacquegna^{145, 146, 147}, M. Sahlén¹⁷⁵, D. B. Sanders⁶³, E. Sarpa^{39, 136, 38}, C. Scarlata¹⁷⁶, J. Schaye⁵⁶, A. Schneider¹⁶², D. Sciotti^{57, 58}, E. Sellentin^{177, 56}, L. C. Smith¹⁷⁸, K. Tanidis¹², G. Testera⁴⁷, R. Teyssier¹⁷⁴, S. Tosi^{46, 47, 34}, A. Troja^{110, 111}, M. Tucci²⁰, C. Valieri¹¹, A. Venhola¹⁷⁹, D. Vergani¹⁰, G. Vernardos^{180, 181}, G. Verza¹⁸², P. Vielzeuf⁷⁴, N. A. Walton¹⁷⁸, J. Wilde¹⁵, and D. Scott¹⁸³

(Affiliations can be found after the references)

June 26, 2025

ABSTRACT

Strong gravitational-lensing systems with multiple source planes are powerful tools for probing the density profiles and dark matter substructure of galaxies. The ratio of the Einstein radii is related to the dark energy equation of state through the cosmological scaling factor β . Galaxy-scale double-source-plane lenses (DSPLs) are extremely rare, however. We report the discovery of four new galaxy-scale DSPL candidates in the Euclid Quick Release 1 (Q1) data. These systems were initially identified through a combination of machine-learning lens-finding models and subsequent visual inspection from citizens and experts. We applied the widely-used LensPop lens-forecasting model to predict that the full *Euclid* survey will discover 1700 DSPLs. This scales to 6 ± 3 DSPLs in 63 deg^2 , which is the area of Q1. The number of discoveries in this work is broadly consistent with this forecast. We present lens models for each DSPL and infer their β values. Our initial Q1 sample demonstrates that *Euclid* promises to discover these rare objects.

Key words. Gravitational lensing: strong – Galaxies: halos – dark matter

1. Introduction

Strong gravitational lensing occurs when a background source and a foreground massive object align along our line of sight, which causes the light from the source to be split into multiple images or to form an Einstein ring (Einstein 1936; Zwicky 1937a,b). There can be multiple sources at different redshifts behind the same lens galaxy at times that form Einstein rings at different radii. These systems are referred to as compound lenses or double-source-plane lenses (DSPLs).

In strong-lensing systems, the radius of the Einstein ring is known as the Einstein radius (parameterised by θ_E) and depends on both the mass profile of the lens and on the cosmological distances that are involved. Lens modelling on systems with a single Einstein ring can constrain the local logarithmic density slope in the region in which the strongly lensed images are observed when a specific parametric form is assumed for the total mass profile of the lens galaxy (e.g., Suyu & Halkola 2010; Birrer & Amara 2018; Nightingale et al. 2021; Galan et al. 2022a). Systematics affect the results, however, such as the mass-sheet degeneracy (Falco et al. 1985; Schneider & Sluse 2013): When a constant mass sheet is added and the convergence is rescaled, mass-sheet transformations (MST) can alter the shape of the galaxy mass profile and rescale the size of the source while keeping all lensing observables unchanged. In DSPL systems, an additional source plane can break the mass-sheet degeneracy of the lens if the mass contribution of the first source is neglected (Bradač et al. 2004) and the cosmology is known.

The presence of two rings at different radii makes DSPLs powerful tools for probing the mass distribution of galaxies, based on which, the properties of dark matter can be constrained. The second ring provides an additional aperture within which the total mass is well constrained, so that we can disentangle the distribution of dark and luminous matter in the lens without additional kinematic data (Sonnenfeld et al. 2012). When a dark matter subhalo exists in the lens plane, the inclusion of a second

source probes the mass distribution on a larger radius. This can break degeneracies in the lens model and improve the constraints on its mass properties (see Figure 6 in Enzi et al. 2024, where the posteriors of the dark matter subhalo when modelled with two arcs are tighter). For example, several observations and analyses of the so-called Jackpot lens SDSS J0946+1006 have suggested the existence of an over-concentrated subhalo (see Vegetti et al. 2010; Minor et al. 2021; Ballard et al. 2024; Despali et al. 2024; Enzi et al. 2024).

The DSPLs have also been used to constrain the equation of state of dark energy. For a system with multiple sources at different redshifts, the ratio of their Einstein radii is related to cosmological parameters such as the dark energy equation of state (parametrised by w) through the cosmology scaling factor β . The cosmological measurements derived from DSPLs are independent of the Hubble constant and complement other cosmological measurements, as demonstrated by previous studies (see e.g., Gavazzi et al. 2008; Collett et al. 2012; Johnson et al. 2025). Collett & Auger (2014) showed that a single galaxy-scale DSPL system can provide competitive cosmological constraints assuming a power-law mass profile of the lens galaxy. Although cluster-scale lenses typically have multiple source planes and are also capable of measuring cosmological parameters (e.g., Soucaill et al. 2004; Jullo et al. 2010; Caminha et al. 2016; Acebron et al. 2017; Magana et al. 2018; Caminha et al. 2022), their complex mass distributions limit the precision. While selecting strong-lensing clusters or galaxy groups with simpler mass distributions is a possible alternative (Bolamperti et al. 2024), galaxy-scale lenses generally exhibit a lower systematic uncertainty due to their inherently simpler mass profiles. Schneider (2014) argued, however, that analogue of the MST exists for DSPL systems that can render the cosmological constraints significantly less restrictive. A 1% bias in β can give rise to a bias in w of approximately 0.3. Additional data from stellar kinematics, for example, can help to break this degeneracy, but competitive results require unbiased measurements of the kinematics

* e-mail: tian.li@port.ac.uk

Table 1. Sky locations are RA and Dec of the four lens systems

Name	RA	Dec
Teapot Lens	273°595	67°138
Cosmic Dartboard	59°565	−50°948
Galileo’s Lens	66°685	−48°111
Cosmic Ammonite	61°239	−49°373

and correct assumptions about the mass profiles. These are both challenging tasks.

Unfortunately, galaxy-scale strong lenses with multiple background sources are exceedingly rare, and only a handful of examples are known in the literature: the Jackpot lens (Gavazzi et al. 2008), the Eye of Horus (Tanaka et al. 2016), and J1721+8842 (Dux et al. 2024). Other DSPLs whose sources have similar Einstein radii are DES0408−5354 (Lin et al. 2017) and the Cosmic Horseshoe (Belokurov et al. 2007). This rarity arises from the fact that whilst the probability of being a single-plane lens scales as θ_E^2 , the probability of lensing two sources scales as θ_E^4 . Even with the depth and resolution of the *Hubble* Space Telescope, only about one in a hundred lenses is expected to be a DSPL (Gavazzi et al. 2008), although the exact rate depends on the depth, resolution, and wavelength of the observations (Collett et al. 2012). The *Euclid* space telescope provides an unprecedented inspection of the sky, and forecasts show that about 1700 DSPLs will be discovered during the survey (rescaling from the 170 000 single-source-plane lenses forecast in Collett 2015).

We report the discovery of four new galaxy-scale DSPL candidates in the 63 deg² of the Euclid Quick Release 1 (Q1 Euclid Quick Release Q1 2025). The I_E -band images and coloured images of the four systems are presented in Fig. 1, and their coordinates are shown in Table 1. Based on the morphology of the four discovered lens systems, they were named Teapot Lens, Cosmic Dartboard, Galileo’s Lens (this lensing configuration somewhat resembles Galileo’s hand-drawn depiction of Saturn), and Cosmic Ammonite.

These four new DSPLs were discovered using the strong-lensing discovery engine, which is a structured workflow that integrates machine learning with citizen-science classifications, followed by expert grading. This paper is part of a series of papers, with Euclid Collaboration: Walmsley et al. (2025) describing the *Euclid* lens-finding engine and new discoveries. Euclid Collaboration: Rojas et al. (2025) describes our effort to build a suitable training sample for Q1 and the lens search with high-velocity dispersion galaxies. Euclid Collaboration: Lines et al. (2025) explains the machine-learning models we used to find the strong lenses. Finally, Euclid Collaboration: Holloway et al. (2025) introduces an ensemble classifier that combines the citizen-science and different machine-learning classifiers.

The paper is organised as follows. In Sect. 2 we briefly summarise the *Euclid* survey and the lens-finding methods we employed. Section 3 introduces the lens-modelling algorithm, followed by the lens models and spectra, which are presented in Sect. 4. In Sect. 5 we present the forecast of the number of DSPLs that *Euclid* will discover in its planned survey area. Finally, Sect. 6 presents our conclusions. We discuss the limitations of our lens-finding approach and provide examples of typical false DSPL systems in Appendix A.

2. Search for a *Euclid* double-source-plane lens

The search for DSPLs is a by-product of the strong-lensing discovery engine, which had the primary goal of finding single-source-plane galaxy-scale strong lenses in *Euclid* data. In the lens-finding pipeline described in Euclid Collaboration: Walmsley et al. (2025), the lens candidates selected by machine-learning and citizen scientists (from objects that are brighter than 22.5 in I_E in the 63 deg² of Q1) are sent to the Galaxy Judges project, where a group of strong-lensing experts provides a final grade for each lens candidate. Following this semi-automated search for all galaxy-galaxy lenses, a group (approximately ten) of experienced experts re-inspected the top 10 000 lenses and identified four DSPLs by eye. All four of our DSPL candidates are ranked in the top 250 lenses by the expert visual inspection.

The primary criterion for identifying a DSPL system are two pairs of arcs at different Einstein radii. The colours of the arcs serve as a key indicator to determine whether they originate from the same source plane. When a lens is identified as a potential DSPL candidate, preliminary lens modelling (described in Sect. 3) is performed to further evaluate the plausibility of its configuration.

Euclid offers significant advantages for DSPL searches due to its high-resolution imaging over a large area. Its point-spread function (PSF) has a full width at half maximum of approximately 0′.16 in the I_E band (Euclid Collaboration: Mellier et al. 2024; Euclid Collaboration: McCracken et al. 2025). This high resolution enables the separation of lens light from the arcs and allows us to resolve multiple arcs. Although the infrared channels have a much lower resolution, their colour information is helpful for associating different arcs.

3. Modelling the double-source-plane lens

3.1. Background theory

For a lensed image at position θ , the scaled deflection angle of a galaxy $\alpha(\theta)$ is related to its lensing potential ψ via

$$\alpha(\theta) = \nabla\psi(\theta), \quad (1)$$

and the relation between lensing potential and lensing convergence is

$$\kappa(\theta) = \frac{1}{2}\nabla^2\psi(\theta), \quad (2)$$

where convergence is defined as

$$\kappa(\theta) \equiv \frac{\Sigma(\theta)}{\Sigma_{\text{cr}}}. \quad (3)$$

The convergence is the surface mass density normalised by the critical lensing surface density,

$$\Sigma_{\text{cr}} \equiv \frac{c^2 D_s}{4\pi G D_l D_{ls}}, \quad (4)$$

where D is the angular diameter distance between two objects, and the subscripts l and s denote the lens galaxy and the source galaxy, respectively.

In a DSPL system, the lens equation of the first source plane can be written as

$$\theta_1 = \theta - \beta\alpha_1(\theta), \quad (5)$$

where α_1 is the reduced deflection angle of the first source at the image position θ , and θ_1 is the position of the first source on its

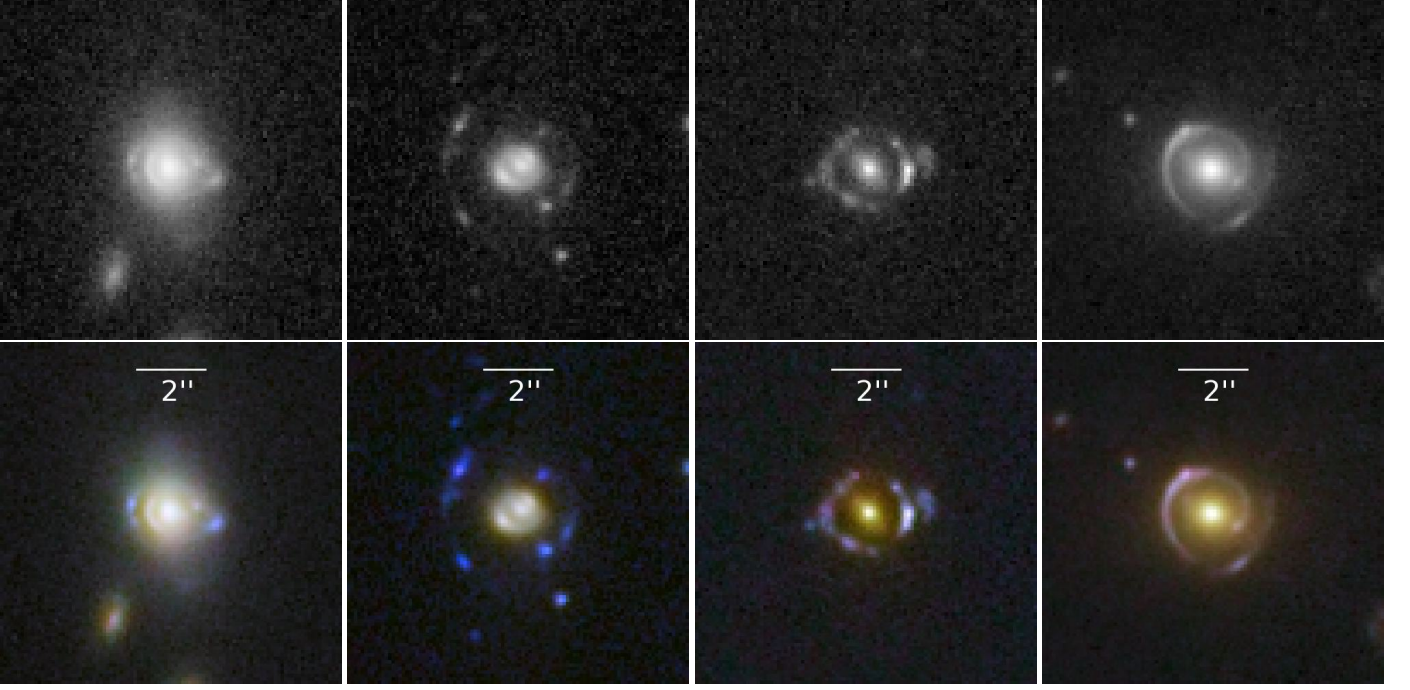


Fig. 1. I_E (top panels) and $I_E-Y_E-J_E$ coloured images (bottom panels) of the DSPL candidates. From left to right, we show Teapot Lens, Cosmic Dartboard, Galileo's Lens, and Cosmic Ammonite. North is up, and east is to the left.

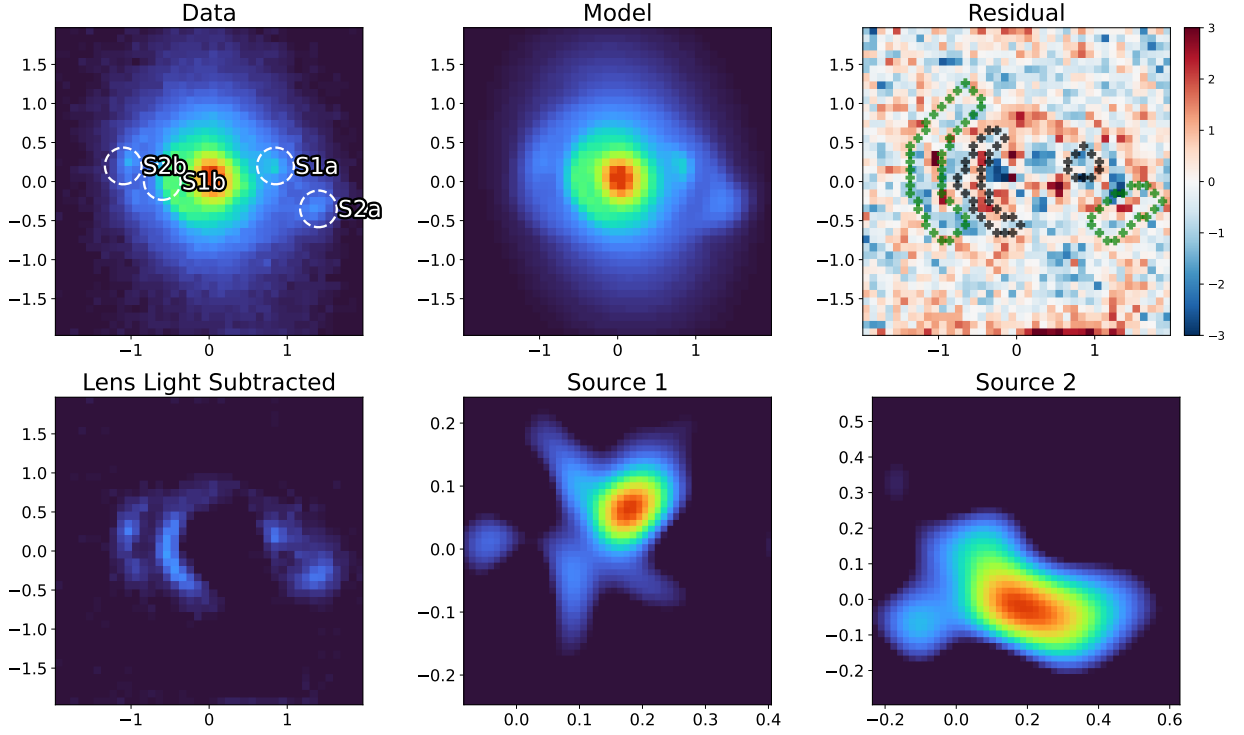


Fig. 2. Lens model of the Teapot Lens. I_E -band image, lens model, and the residual. The bottom panels display the lens light-subtracted image and two source models. The inner pair of arcs is labelled S1a and S1b, and the outer pair of arcs is labelled S2a and S2b. In the residual plot, the black and green scatter points represent the edges of the masks for the inner and outer arcs, respectively (we did not use the arc mask in our modelling). The axis tick marks are in arcseconds.

source plane. Here, β is the cosmological scaling factor, which is the ratio of the angular diameter distances between the different redshift planes,

$$\beta = \frac{D_{ls1}D_{s2}}{D_{s1}D_{ls2}},$$

where the subscripts s1 and s2 denote source 1 and source 2, respectively. The lens equation of the second source plane is then

$$(6) \quad \theta_2 = \theta - \alpha_1(\theta) - \alpha_{s1}[\theta - \beta \alpha_1(\theta)], \quad (7)$$

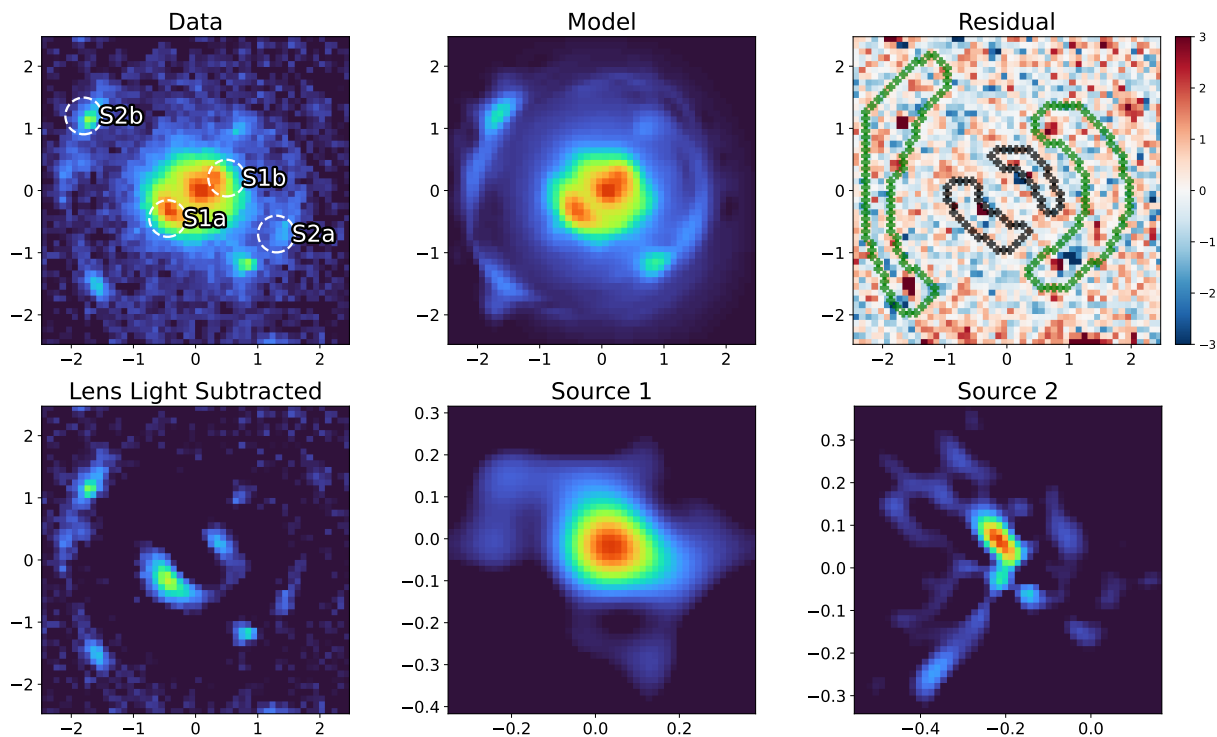


Fig. 3. Same as Fig. 2, but for Cosmic Dartboard.

where θ_2 is the position of the second source on its source plane, and α_{s1} is the deflection angle of the mass on the first source plane. In a simple case for which we assume that the lens galaxy has a singular isothermal sphere (SIS) profile, the parameter β is just the ratio of the two Einstein radii (the geometry of the DSPL is in Figure 1 of Collett & Auger 2014).

The lenses are modelled using an elliptical power-law (EPL) mass model with an external shear component. The convergence (κ_{EPL}) of the EPL model can be parametrised as

$$\kappa_{\text{EPL}}(\rho, \gamma, q) = \frac{3 - \gamma}{2} \left(\frac{\theta_E}{\rho} \right)^{\gamma-1}, \quad (8)$$

where $\rho^2 = x^2q + y^2/q$ is the squared elliptical radius, and q is the axis ratio, γ is the power-law index of the density slope, and θ_E is the Einstein radius. We used θ_{E1} to represent the Einstein radius of the primary lens with respect to source 1, θ_{E2} for the Einstein radius of the same lens with respect to source 2 (with source 1 absent), and θ_{sis1} for the Einstein radius when source 1 itself lensed source 2. The cosmological parameters can therefore be measured by relating β from the lens modelling and the redshifts of the system.

3.2. Lens modelling strategy

We used the open-source lens modelling code *Hercules*¹ (Galan et al. 2022b), which now includes multiplane lensing capabilities (see, e.g. Enzi et al. (2024)). *Hercules* is based on the automatic differentiation and compilation features of JAX² and can run on graphics processing units (GPUs). We note here that our lens modelling primarily aims to validate that these systems are plausible DSPLs, and we do not infer the parameters of these systems precisely. The lack of redshift information

for either the lens or the sources prevents us from building a robust mass distribution and leverage the full statistical analyses from Markov chain Monte Carlo (MCMC) methods. Our lens modelling is fully capable of recovering the source-plane morphology of the galaxies in order to confirm the double-source-plane nature of the systems, however. We briefly summarise the modelling strategy.

The data we used for the modelling came from the I_E band because it has the highest pixel resolution ($0''.1 \text{ pixel}^{-1}$). We measured the root mean square of the background pixels and inferred the shot noise from the modelled lens light. The PSF was derived from the *Euclid* pipeline. Since the *Euclid* I_E band spans a wide wavelength range (550–900 nm), the PSF profile will be influenced by the spectral energy distribution of the target. Consequently, lensed arcs with markedly different colours might exhibit different PSFs, which might introduce additional uncertainties into the lens model.

We used the *Numpyro* implementation of stochastic variational inference (SVI; see Wingate & Weber 2013). We employed the *AdaBelief* optimiser (Zhuang et al. 2020) with a low-rank multivariate normal distribution as the guiding probability distribution. This guiding distribution is not complex enough to accurately recover the full posterior distribution, but it is computationally much cheaper than MCMC methods because it can use the auto-differentiable nature of JAX (Bradbury et al. 2018). The inference was made through optimising the guiding distribution to minimise the Kullback–Leibler divergence to the true posterior rather than sampling over the posterior.

Since the inner arcs of our DSPL candidates are mixed with the lens light, we modelled the lens light simultaneously with the arcs. In our model, the lens light was modelled with the sum of five elliptical Gaussian luminosity profiles with flexible centres (Shajib 2019; He et al. 2024; Enzi et al. 2024). The sources were first modelled with a single elliptical Gaussian luminosity profile to provide an approximate answer. Then, we used the

¹ <https://github.com/Hercules/hercules>

² <https://docs.jax.dev/en/latest/>

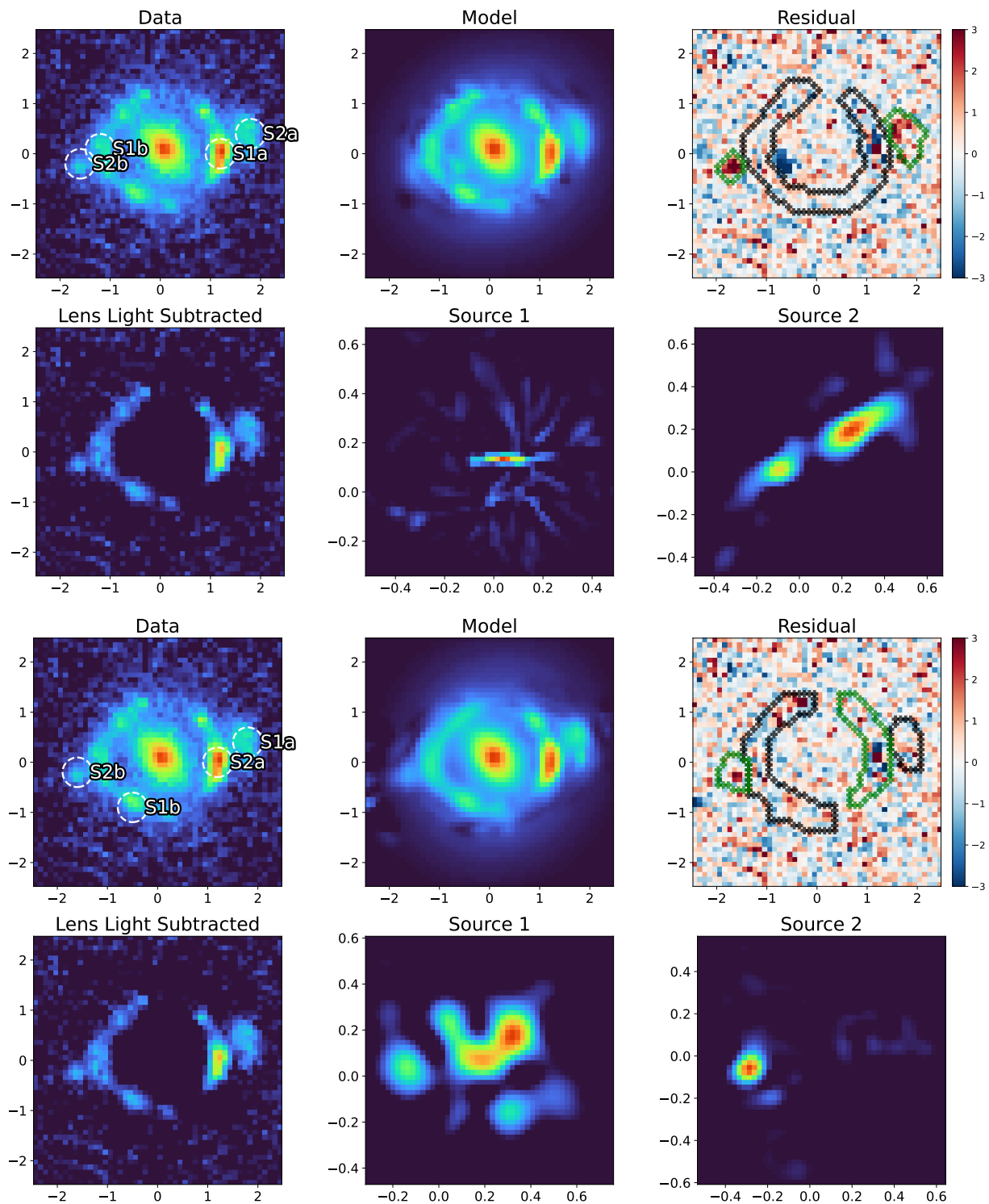


Fig. 4. Same as Fig. 2, but for Galileo's Lens. The top six panels show the lens modelled with a single-source plane. The bottom six panels show the lens modelled with double-source-planes.

parametrised lens model as the starting point and described the sources as fields that vary on regularly pixelated grids. The pixelated source was regularised by multiplying the square root of the Matérn power spectrum (see Stein 2012) with white noise (sampled from a standard normal distribution) and then applying the inverse-Fourier transform to the result. A flat prior was applied to every mass model parameter.

For each of our targets, we ran 20 000 iterations in 10 SVIs. Each SVI realisation had different random initialisations, and we chose the SVI result with the lowest average loss value to be our lens model. The lens model results are shown in Table 2. We do not show the uncertainty of the lens model because SVI tends to underestimate the lens model uncertainty. The expected uncertainties from the subsequent MCMCs are typically about 0.05 for each parameter.

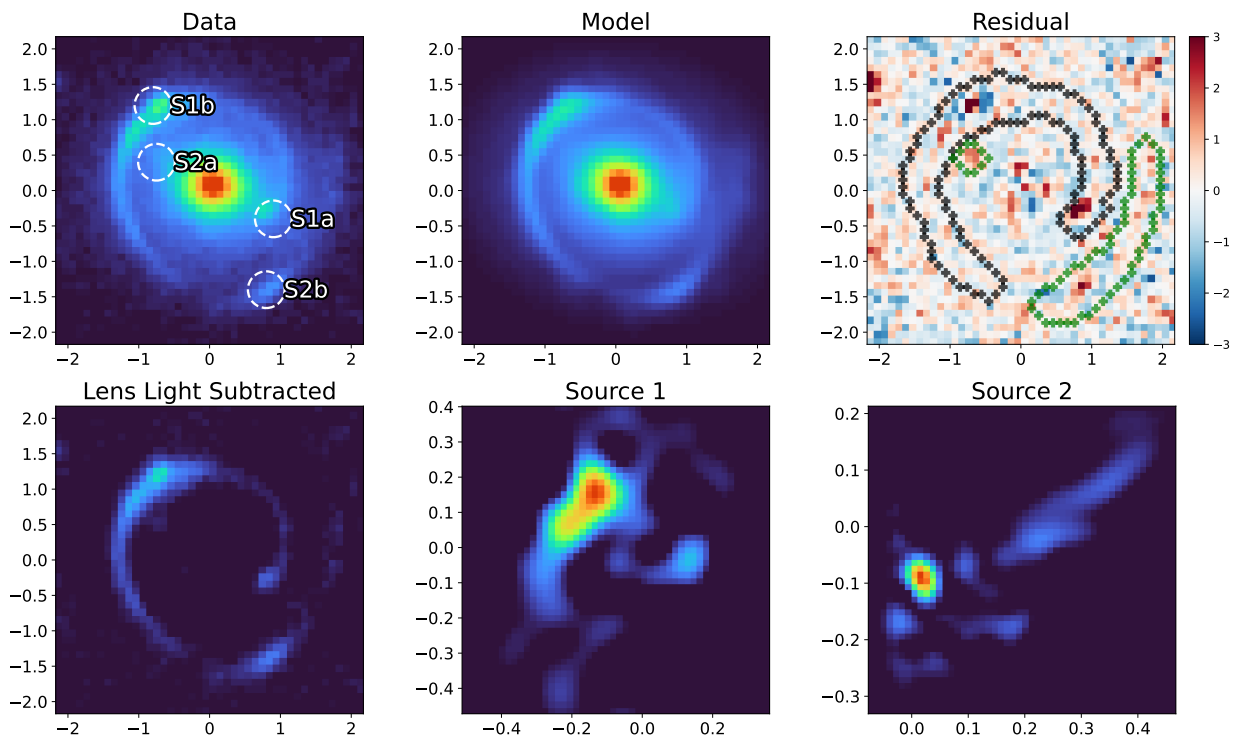


Fig. 5. Same as Fig. 2, but for Cosmic Ammonite.

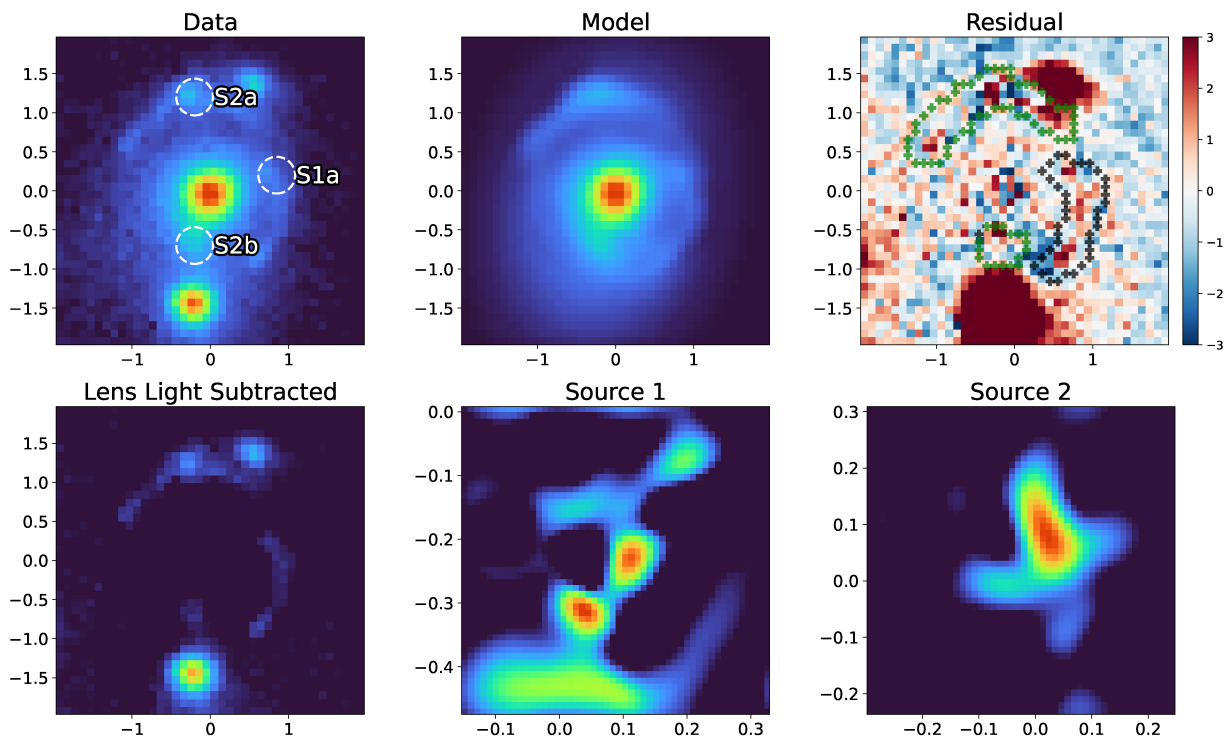


Fig. 6. Same as Fig. 2, but for the Crackpot lens.

4. Lens model of DSPL candidates

In this section, we present and analyse the lens models of our DSPL candidates (Teapot Lens, Cosmic Dartboard, Galileo’s Lens, and Cosmic Ammonite). We also present one system that we initially thought was a DSPL candidate, the Crackpot, which we found was better modelled with two sources on a single plane

(Sect 4.5). Since the Crackpot is not a DSPL lens, it is not shown in Table 2.

4.1. Teapot Lens

This lens was discovered during the visual inspection of the top 20 000 ranked lenses according to the lens-finding version of the machine-learning model Zoobot (see [Euclid Collaboration: Lines et al. 2025](#)). It was ranked 2349 by Zoobot and 43 in Galaxy Judges. It was classified as a grade A lens. The system features two concentric rings at distinct Einstein radii, each with a different colour. This means that it is a highly promising DSPL candidate.

The lens model of Teapot Lens is presented in Fig. 2. The lens light-subtracted image reveals a distinct pair of inner rings. The results of the lens model indicate an inner ring at $0''.62$ and a β of 0.74, leaving a clean residual within the arc position. The positive residual near the centre might be due to multiple reasons, such as dust lanes or an AGN in the lens galaxy; a PSF mismatch that affects the lens light subtraction; a satellite galaxy located close to the primary lens; or an inner zig-zag image of the second source ([Collett & Bacon 2016](#)).

4.2. Cosmic Dartboard

This lens was discovered during the visual inspection of the top 20 000 ranked lenses. It ranked 1902 by Zoobot and 94 in Galaxy Judges. It was classified as a grade A lens. The lens model of the Cosmic Dartboard is presented in Fig. 3. Our lens model successfully recovered all the details in the image. Because the resolution is limited, however, it is challenging to perfectly distinguish the lens light from the inner arc. The reconstruction of the outer arc might be significantly improved with data with a higher signal-to-noise ratio.

The inner ring of this lens was inferred to be at $0''.45$, while the β value is 0.51. The first source is massive according to the result from the lens model ($\theta_{\text{sis1}} = 0''.48$) because it appears to be an elliptical galaxy. If spectroscopic redshifts are obtained, the large Einstein radius ratio should provide valuable insights for cosmological measurements as the image configuration suggests $z_{s1} \ll z_{s2}$, which would provide the optical lever arm for constraining dark energy ([Collett et al. 2012](#)).

4.3. Galileo's Lens

This lens was first discovered in Space Warps and Galaxy Judges. It ranked 3 by Zoobot (although it was missed as a DSPL candidate in the first pass of Zoobot by TC, TL, and NL) and 19 in Galaxy Judges. It was classified as a grade A lens. This system was proposed as a DSPL system because it features a central ring structure and two faint arcs in the outskirts. The apparent inner ring has an unusual configuration, however, and the colours of all the arcs are similar. This makes it difficult to classify the source confidently. It is also difficult to explain the highly elliptical central lens light and the nearly circular ring by merely classifying it as a ring galaxy.

We present two lens models. The first model assumed a DSPL configuration, and the second model considered a lens with two sources situated on the same redshift plane. Neither model can explain the lensing configuration really well. This system might be a single ring system in which the two blue objects nearby are just field galaxies. Spectroscopic data or imaging with a higher resolution should provide definitive evidence to decide whether this system is indeed a DSPL.

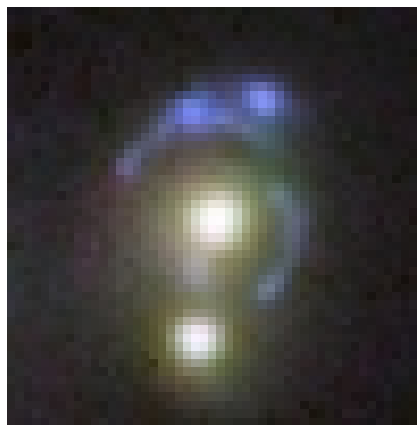


Fig. 7. Colour image of the Crackpot lens.

4.4. Cosmic Ammonite

This lens was discovered during the visual inspection of the top 1000 Galaxy Judges candidates. It ranked 7 in Zoobot (but was initially assumed to be a multi-component single-source plane system) and 207 in Galaxy Judges. It was classified as a grade B lens, but the expert scores were not unanimous, with four A* votes (lens with special interest), one A vote, three B votes, and two X votes (non-lens).

The lens model of Cosmic Ammonite is presented in Fig. 5. Our lens model successfully recovered all the details in the image. The β of this system is constrained to be around 0.85. Although this system was modelled with excellent fidelity and is almost certainly a DSPL, it received a surprisingly low score in Galaxy Judges. The best explanation is that the lensing configuration of this system is uncommon, so that human experts are less confident about this object. We initially modelled this system with the expectation that it would be ruled out as a DSPL, with the two sources on a single plane. The modelling result shows, however, that this is a confident DSPL with $\beta \approx 0.85$. This demonstrates the power of lens modelling over human experts in identifying DSPLs with β not much smaller than one.

4.5. The Crackpot: A single-plane system with two sources

This lens was first discovered during the visual inspection of high-velocity dispersion galaxies from the Dark Energy Spectroscopic Instrument ([Euclid Collaboration: Rojas et al. 2025](#)) as part of the effort to build a training set for machine learning. It was later rediscovered in Space Warps and Galaxy Judges, ranking 622 in the Zoobot and 237 in Galaxy Judges. It was classified as a grade B lens. As shown in Fig. 7, the system features two blue arcs at different radii. It is a lens with two bright lensing elliptical galaxies. While the counter-image of the top arc is clearly visible in the bottom left corner of the lens, the counter-image of the inner arc is only faintly visible in the lens light-subtracted image. Its identification is therefore less convincing.

Figure 6 shows the lens model of the Crackpot lens. If the faint inner arc is real, the double-source-plane lens model suggests that the two images have similar Einstein radii. The nearby galaxy at the bottom of the image complicates the mass profile, however. For simplicity, we did not include the mass of the southern galaxy, and we masked the blue blob in the top right corner of the northern source. Based on these factors, this lens is probably not a DSPL, but rather a lens with two sources at the same redshift. We named this system the Crackpot as a tongue-

Table 2. Properties and lens model parameters of the four systems.

Name	I_E (lens)	I_E (s1)	I_E (s2)	β	θ_{E1}	θ_{sis1}	θ_{E2}	γ	ϕ	q
Teapot Lens	20.0	23.3	24.0	0.74	0''.62	0''.13	0''.89	1.83	-0.44	0.63
Cosmic Dartboard	21.2	22.9	23.2	0.51	0''.45	0''.48	1''.31	1.63	-1.32	0.64
Galileo's Lens	22.3	22.7	24.4	0.69	1''.09	0''.28	1''.52	2.11	0.39	0.76
Cosmic Ammonite	20.0	22.3	24.2	0.85	1''.18	0''.15	1''.35	2.22	0.17	0.72

Notes. We show the lensed I_E -band magnitudes of the lens, source 1 (s1), and source 2 (s2). The lens model parameters are the best solutions after 10 SVI runs per lens. The uncertainties are typically around 0.05 for each parameter from subsequent MCMCs.

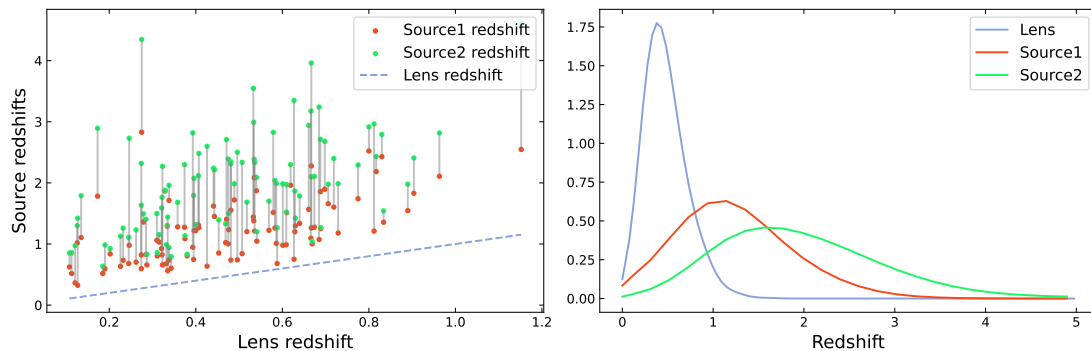


Fig. 8. *Left:* Redshift distribution of 100 example DSPLs from LensPop. *Right:* Histogram of the redshift distribution of 1700 systems drawn from LensPop. The blue line indicates the lens redshift, and the dashed red and green lines mark the redshifts of source 1 and source 2, respectively.

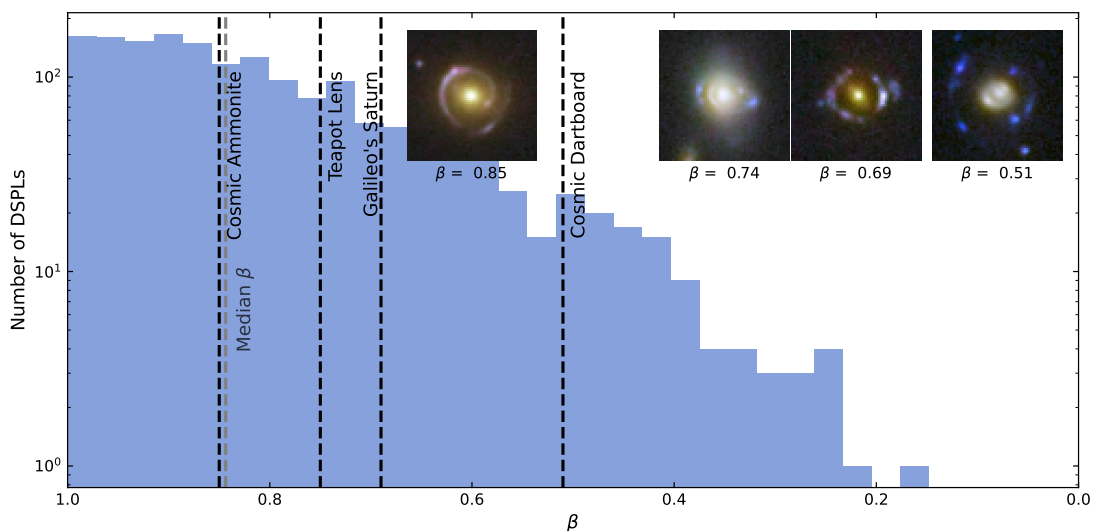


Fig. 9. Distribution of β from the forecast. The dashed black lines mark the measured β values for DSPLs discovered in Q1, and the dashed grey line indicates the median β value in the forecast catalogue.

in-cheek reference to the fact it is not a Jackpot lens after all. A more definitive judgement will require higher-resolution imaging observations and spectral information.

5. Expected rate and population of DSPLs in Euclid

The *Euclid* survey is expected to enable the construction of a sample of approximately 1700 galaxy-scale DSPL systems. This forecast is derived from the LensPop package (Collett 2015), modified to include multiple background sources (we neglected the mass of the first source). We also imposed more stringent constraints than the LensPop defaults. Specifically, we required

that both sources have one or more arcs with a length of $0''.3$, which ensured that the density slope of the lens can be recovered from *Euclid* imaging alone with a reasonably high possibility. The redshift distribution for lenses and sources is shown in Fig. 8. Although most compound lenses are at $z \approx 0.5$, a significant fraction of the lenses are at $z < 0.2$ and at $z > 1$, which is promising for a precise constraint on the mass distribution in lenses. Of the 1700 expected *Euclid* DSPLs, approximately 6 ± 3 should fall inside the Q1 footprint (assuming that the DSPLs are distributed randomly). The entire *Euclid* survey will cover about $14\,000 \text{ deg}^2$, whereas the Q1 footprint we considered spans only 63 deg^2 . The forecast number of systems in

this small area is expected to be modest, and even a difference of a few lenses (e.g. finding four instead of the predicted six) can therefore be attributed to small-number statistics. Poisson fluctuations and cosmic variance can easily shift the observed number by a few systems relative to theoretical forecasts.

Our four DSPLs already more than double the galaxy-galaxy DSPL population. This is expected to be useful for cosmography, but without any redshift information, it is impossible to map β values onto cosmological parameter constraints. Notably, Cosmic Dartboard has $\beta \approx 0.51$, which is quite rare based on the β distribution of the mock catalogue, as shown in Fig. 9 (only 6% of the DSPLs have $\beta < 0.5$, and the probability of having at least one DSPL with $\beta < 0.5$ in four systems therefore is 0.2). This indicates that our forecast might underestimate the DSPL population observed by *Euclid*. Theoretically, lower β values (two source galaxies at very different redshift) are more sensitive to the cosmology parameters because a DSPL with a decreased β provides a stronger geometric leverage and mitigates degeneracies among the cosmological parameters. For instance, when $\beta \approx 1$ ($z_{s1} \approx z_{s2}$), variations in cosmological parameters may cause β to remain close to one.

6. Conclusions

We have identified four new galaxy-scale DSPL candidates in Q1. This significantly extends the limited sample of known DSPL systems. Our detailed lens modelling again showed that they probably are DSPLs, and we derived the β parameters (the cosmological scaling factor that represents the distance ratio) for each candidate, which demonstrates that they can be used in cosmological studies. For a handful of DSPL candidates, higher-resolution imaging and spectroscopic redshifts are needed for a definitive conclusion about their nature.

We employed the single-source plane lens search to find interesting DSPL candidates. We did not train any machine or human classifiers to explicitly search for DSPLs. One consequence of not creating machine-learning lens-finders trained on DSPLs is that they do not learn to value DSPL systems higher than regular lenses. This means that the DSPLs will not necessarily be ranked exceptionally highly among the lenses; this was found in Q1 (Euclid Collaboration: Lines et al. 2025). Future *Euclid* single-plane lens searches will be made over larger areas, which means that we will be unable to visually inspect the same proportion of the total sample as in Q1: The proportion of the total number of images that were visually inspected in Q1 scaled up to the full *Euclid* survey would correspond to visually inspecting six million images, which is likely intractable. The DSPLs and the single-source-plane lenses found in Q1 will likely enable a significant improvement in the machine-learning performance, and the training of machine-learning models on DSPLs will increase the probability that they are recovered in future *Euclid* lens searches. A dedicated DSPL search might be needed for *Euclid* DR1 and beyond, however.

Some DSPLs may still remain to be found in Q1, either because they were ranked poorly by the single-source-plane lens machine-learning classifiers or because they were missed in the visual inspection (we do not yet know how our method performs with systems with a small Einstein radius). We also missed any lenses that did not pass our initial lens cuts ($I_E < 22.5$). Some lenses are expected to be faint in I_E ($I_E > 24$, Collett 2015), although these would typically be low-mass or high-redshift lenses (e.g. a lens redshift higher than 1.5). Either scenario is less likely to produce a *Euclid*-detectable DSPL than a galaxy that is more luminous in I_E . Our forecasts indicate that the full *Euclid* sur-

vey at the end of operations is expected to uncover 1700 DSPLs, whilst extrapolating up from our four DSPLs in 63 deg² yields 1000 (± 500) DSPLs in the full survey. Regardless of whether we ultimately find 1000 or 1700 lenses in the full *Euclid* data set, it is already clear that *Euclid* will revolutionise the research made using DSPLs.

Acknowledgements. Numerical computations were done on the Sciama High Performance Compute (HPC) cluster, which is supported by the ICG, SEPNet, and the University of Portsmouth. This work has received funding from the European Research Council (ERC) under the European Union's Horizon 2020 research and innovation program (LensEra: grant agreement No 945536). TC is funded by the Royal Society through a University Research Fellowship. CT acknowledges the INAF grant 2022 LEMON. For the purpose of open access, the authors have applied a Creative Commons Attribution (CC BY) license to any Author Accepted Manuscript version arising. The Euclid Consortium acknowledges the European Space Agency and a number of agencies and institutes that have supported the development of *Euclid*, in particular the Agenzia Spaziale Italiana, the Austrian Forschungsförderungsgesellschaft funded through BMK, the Belgian Science Policy, the Canadian Euclid Consortium, the Deutsches Zentrum für Luft- und Raumfahrt, the DTU Space and the Niels Bohr Institute in Denmark, the French Centre National d'Etudes Spatiales, the Fundação para a Ciência e a Tecnologia, the Hungarian Academy of Sciences, the Ministerio de Ciencia, Innovación y Universidades, the National Aeronautics and Space Administration, the National Astronomical Observatory of Japan, the Nederlandse Onderzoeksschool Voor Astronomie, the Norwegian Space Agency, the Research Council of Finland, the Romanian Space Agency, the State Secretariat for Education, Research, and Innovation (SERI) at the Swiss Space Office (SSO), and the United Kingdom Space Agency. A complete and detailed list is available on the *Euclid* web site (www.euclid-ec.org).

7. Data Availability

The Q1 data is available at the *Euclid* science archive. The forecast population of DSPLs are available at LensPop github repository. The derived data products are available upon request from the corresponding author.

References

- Acebron, A., Jullo, E., Limousin, M., et al. 2017, MNRAS, 470, 1809
- Ballard, D. J., Enzi, W. J. R., Collett, T. E., Turner, H. C., & Smith, R. J. 2024, MNRAS, 528, 7564
- Belokurov, V., Evans, N. W., Moiseev, A., et al. 2007, ApJ, 671, L9
- Birrer, S. & Amara, A. 2018, Physics of the Dark Universe, 22, 189
- Bolamperti, A., Grillo, C., Caminha, G. B., et al. 2024, A&A, 692, A239
- Bradač, M., Lombardi, M., & Schneider, P. 2004, A&A, 424, 13
- Bradbury, J., Frostig, R., Hawkins, P., et al. 2018, JAX: composable transformations of Python+NumPy programs
- Caminha, G. B., Grillo, C., Rosati, P., et al. 2016, A&A, 587, A80
- Caminha, G. B., Suyu, S. H., Grillo, C., & Rosati, P. 2022, A&A, 657, A83
- Collett, T. E. 2015, ApJ, 811, 20
- Collett, T. E. & Auger, M. W. 2014, MNRAS, 443, 969
- Collett, T. E., Auger, M. W., Belokurov, V., Marshall, P. J., & Hall, A. C. 2012, MNRAS, 424, 2864
- Collett, T. E. & Bacon, D. J. 2016, MNRAS, 456, 2210
- Despali, G., Heinze, F. M., Fassnacht, C. D., et al. 2024, arXiv e-prints, arXiv:2407.12910
- Dux, F., Millon, M., Lemon, C., et al. 2024, arXiv e-prints, arXiv:2411.04177
- Einstein, A. 1936, Science, 84, 506
- Enzi, W. J. R., Krawczyk, C. M., Ballard, D. J., & Collett, T. E. 2024, arXiv e-prints, arXiv:2411.08565
- Euclid Collaboration: Holloway, P., Verma, A., Walmsley, M., et al. 2025, A&A, submitted, (Euclid Q1 SI)
- Euclid Collaboration: Lines, N. E. P., Collett, T. E., Walmsley, M., et al. 2025, A&A, submitted, (Euclid Q1 SI)
- Euclid Collaboration: McCracken, H., Benson, K., et al. 2025, A&A, submitted, (Euclid Q1 SI)
- Euclid Collaboration: Mellier, Y., Abdurro'uf, Acevedo Barroso, J., et al. 2024, A&A, accepted, arXiv:2405.13491
- Euclid Collaboration: Rojas, K., Collett, T., Acevedo Barroso, J., et al. 2025, A&A, submitted, (Euclid Q1 SI)
- Euclid Collaboration: Walmsley, M., Holloway, P., Lines, N., et al. 2025, A&A, submitted, (Euclid Q1 SI)

- Euclid Quick Release Q1. 2025, <https://doi.org/10.57780/esa-2853f3b>, (Euclid Q1 SI)
- Falco, E. E., Gorenstein, M. V., & Shapiro, I. I. 1985, *ApJ*, 289, L1
- Galan, A., Vernardos, G., Peel, A., Courbin, F., & Starck, J. L. 2022a, *A&A*, 668, A155
- Galan, A., Vernardos, G., Peel, A., Courbin, F., & Starck, J. L. 2022b, *A&A*, 668, A155
- Gavazzi, R., Treu, T., Koopmans, L. V. E., et al. 2008, *ApJ*, 677, 1046
- He, Q., Nightingale, J. W., Amvrosiadis, A., et al. 2024, *MNRAS*, 532, 2441
- Johnson, D., Collett, T., Li, T., & Fleury, P. 2025, arXiv e-prints, arXiv:2501.17153
- Jullo, E., Natarajan, P., Kneib, J. P., et al. 2010, *Science*, 329, 924
- Lin, H., Buckley-Geer, E., Agnello, A., et al. 2017, *ApJ*, 838, L15
- Magana, J., Acebron, A., Motta, V., et al. 2018, *ApJ*, 865, 122
- Minor, Q. E., Gad-Nasr, S., Kaplinghat, M., & Vegetti, S. 2021, *MNRAS*, 507, 1662
- Nightingale, J., Hayes, R., Kelly, A., et al. 2021, *The Journal of Open Source Software*, 6, 2825
- Schneider, P. 2014, *A&A*, 568, L2
- Schneider, P. & Sluse, D. 2013, *A&A*, 559, A37
- Shajib, A. J. 2019, *MNRAS*, 488, 1387
- Sonnenfeld, A., Treu, T., Gavazzi, R., et al. 2012, *ApJ*, 752, 163
- Soucail, G., Kneib, J. P., & Golse, G. 2004, *A&A*, 417, L33
- Stein, M. 2012, *Interpolation of Spatial Data: Some Theory for Kriging*, Springer Series in Statistics (Springer New York)
- Suyu, S. H. & Halkola, A. 2010, *A&A*, 524, A94
- Tanaka, M., Wong, K. C., More, A., et al. 2016, *ApJ*, 826, L19
- Vegetti, S., Koopmans, L. V. E., Bolton, A., Treu, T., & Gavazzi, R. 2010, *MNRAS*, 408, 1969
- Wingate, D. & Weber, T. 2013, arXiv e-prints, arXiv:1301.1299
- Zhuang, J., Tang, T., Ding, Y., et al. 2020, arXiv e-prints, arXiv:2010.07468
- Zwicky, F. 1937a, *Phys. Rev.*, 51, 290
- Zwicky, F. 1937b, *Phys. Rev.*, 51, 679
- ¹⁹ SCITAS, Ecole Polytechnique Fédérale de Lausanne (EPFL), 1015 Lausanne, Switzerland
- ²⁰ Department of Astronomy, University of Geneva, ch. d'Ecogia 16, 1290 Versoix, Switzerland
- ²¹ Max-Planck-Institut für Astrophysik, Karl-Schwarzschild-Str. 1, 85748 Garching, Germany
- ²² Technical University of Munich, TUM School of Natural Sciences, Physics Department, James-Franck-Str. 1, 85748 Garching, Germany
- ²³ Departamento Física Aplicada, Universidad Politécnica de Cartagena, Campus Muralla del Mar, 30202 Cartagena, Murcia, Spain
- ²⁴ School of Physical Sciences, The Open University, Milton Keynes, MK7 6AA, UK
- ²⁵ STAR Institute, University of Liège, Quartier Agora, Allée du six août 19c, 4000 Liège, Belgium
- ²⁶ INAF-Osservatorio Astronomico di Capodimonte, Via Moiriarillo 16, 80131 Napoli, Italy
- ²⁷ Department of Physics, Institute for Computational Cosmology, Durham University, South Road, Durham, DH1 3LE, UK
- ²⁸ Department of Physics, Centre for Extragalactic Astronomy, Durham University, South Road, Durham, DH1 3LE, UK
- ²⁹ The Inter-University Centre for Astronomy and Astrophysics, Post Bag 4, Ganeshkhind, Pune 411007, India
- ³⁰ Kavli Institute for the Physics and Mathematics of the Universe (WPI), University of Tokyo, Kashiwa, Chiba 277-8583, Japan
- ³¹ Université Paris-Saclay, CNRS, Institut d'astrophysique spatiale, 91405, Orsay, France
- ³² ESAC/ESA, Camino Bajo del Castillo, s/n., Urb. Villafranca del Castillo, 28692 Villanueva de la Cañada, Madrid, Spain
- ³³ School of Mathematics and Physics, University of Surrey, Guildford, Surrey, GU2 7XH, UK
- ³⁴ INAF-Osservatorio Astronomico di Brera, Via Brera 28, 20122 Milano, Italy
- ³⁵ Université Paris-Saclay, Université Paris Cité, CEA, CNRS, AIM, 91191, Gif-sur-Yvette, France
- ³⁶ IFPU, Institute for Fundamental Physics of the Universe, via Beirut 2, 34151 Trieste, Italy
- ³⁷ INAF-Osservatorio Astronomico di Trieste, Via G. B. Tiepolo 11, 34143 Trieste, Italy
- ³⁸ INFN, Sezione di Trieste, Via Valerio 2, 34127 Trieste TS, Italy
- ³⁹ SISSA, International School for Advanced Studies, Via Bonomea 265, 34136 Trieste TS, Italy
- ⁴⁰ Dipartimento di Fisica e Astronomia, Università di Bologna, Via Gobetti 93/2, 40129 Bologna, Italy
- ⁴¹ INAF-Osservatorio Astronomico di Padova, Via dell'Osservatorio 5, 35122 Padova, Italy
- ⁴² Max Planck Institute for Extraterrestrial Physics, Giessenbachstr. 1, 85748 Garching, Germany
- ⁴³ Universitäts-Sternwarte München, Fakultät für Physik, Ludwig-Maximilians-Universität München, Scheinerstrasse 1, 81679 München, Germany
- ⁴⁴ Institut de Physique Théorique, CEA, CNRS, Université Paris-Saclay 91191 Gif-sur-Yvette Cedex, France
- ⁴⁵ Space Science Data Center, Italian Space Agency, via del Politecnico snc, 00133 Roma, Italy
- ⁴⁶ Dipartimento di Fisica, Università di Genova, Via Dodecaneso 33, 16146, Genova, Italy
- ⁴⁷ INFN-Sezione di Genova, Via Dodecaneso 33, 16146, Genova, Italy
- ⁴⁸ Department of Physics "E. Pancini", University Federico II, Via Cinthia 6, 80126, Napoli, Italy
- ⁴⁹ Instituto de Astrofísica e Ciências do Espaço, Universidade do Porto, CAUP, Rua das Estrelas, PT4150-762 Porto, Portugal
- ⁵⁰ Faculdade de Ciências da Universidade do Porto, Rua do Campo de Alegre, 4150-007 Porto, Portugal
- ⁵¹ Dipartimento di Fisica, Università degli Studi di Torino, Via P. Giuria 1, 10125 Torino, Italy
- ⁵² INFN-Sezione di Torino, Via P. Giuria 1, 10125 Torino, Italy
- ⁵³ INAF-Osservatorio Astrofisico di Torino, Via Osservatorio 20, 10025 Pino Torinese (TO), Italy
- ¹ Institute of Cosmology and Gravitation, University of Portsmouth, Portsmouth PO1 3FX, UK
- ² David A. Dunlap Department of Astronomy & Astrophysics, University of Toronto, 50 St George Street, Toronto, Ontario M5S 3H4, Canada
- ³ Jodrell Bank Centre for Astrophysics, Department of Physics and Astronomy, University of Manchester, Oxford Road, Manchester M13 9PL, UK
- ⁴ University of Applied Sciences and Arts of Northwestern Switzerland, School of Engineering, 5210 Windisch, Switzerland
- ⁵ School of Mathematics, Statistics and Physics, Newcastle University, Herschel Building, Newcastle-upon-Tyne, NE1 7RU, UK
- ⁶ Jet Propulsion Laboratory, California Institute of Technology, 4800 Oak Grove Drive, Pasadena, CA, 91109, USA
- ⁷ Aix-Marseille Université, CNRS, CNES, LAM, Marseille, France
- ⁸ Institut d'Astrophysique de Paris, UMR 7095, CNRS, and Sorbonne Université, 98 bis boulevard Arago, 75014 Paris, France
- ⁹ Dipartimento di Fisica e Astronomia "Augusto Righi" - Alma Mater Studiorum Università di Bologna, via Piero Gobetti 93/2, 40129 Bologna, Italy
- ¹⁰ INAF-Osservatorio di Astrofisica e Scienza dello Spazio di Bologna, Via Piero Gobetti 93/3, 40129 Bologna, Italy
- ¹¹ INFN-Sezione di Bologna, Viale Berti Pichat 6/2, 40127 Bologna, Italy
- ¹² Department of Physics, Oxford University, Keble Road, Oxford OX1 3RH, UK
- ¹³ Dipartimento di Fisica "Aldo Pontremoli", Università degli Studi di Milano, Via Celoria 16, 20133 Milano, Italy
- ¹⁴ INAF-IASF Milano, Via Alfonso Corti 12, 20133 Milano, Italy
- ¹⁵ Institut de Ciències del Cosmos (ICCUB), Universitat de Barcelona (IEEC-UB), Martí i Franqués 1, 08028 Barcelona, Spain
- ¹⁶ Institució Catalana de Recerca i Estudis Avançats (ICREA), Passeig de Luíís Companys 23, 08010 Barcelona, Spain
- ¹⁷ Sydney Institute for Astronomy, School of Physics, University of Sydney, NSW 2006, Australia
- ¹⁸ Institute of Physics, Laboratory of Astrophysics, Ecole Polytechnique Fédérale de Lausanne (EPFL), Observatoire de Sauverny, 1290 Versoix, Switzerland

- ⁵⁴ European Space Agency/ESTEC, Keplerlaan 1, 2201 AZ Noordwijk, The Netherlands
- ⁵⁵ Institute Lorentz, Leiden University, Niels Bohrweg 2, 2333 CA Leiden, The Netherlands
- ⁵⁶ Leiden Observatory, Leiden University, Einsteinweg 55, 2333 CC Leiden, The Netherlands
- ⁵⁷ INAF-Osservatorio Astronomico di Roma, Via Frascati 33, 00078 Monteporzio Catone, Italy
- ⁵⁸ INFN-Sezione di Roma, Piazzale Aldo Moro, 2 - c/o Dipartimento di Fisica, Edificio G. Marconi, 00185 Roma, Italy
- ⁵⁹ Centro de Investigaciones Energéticas, Medioambientales y Tecnológicas (CIEMAT), Avenida Complutense 40, 28040 Madrid, Spain
- ⁶⁰ Port d'Informació Científica, Campus UAB, C. Albareda s/n, 08193 Bellaterra (Barcelona), Spain
- ⁶¹ Institute for Theoretical Particle Physics and Cosmology (TTK), RWTH Aachen University, 52056 Aachen, Germany
- ⁶² INFN section of Naples, Via Cinthia 6, 80126, Napoli, Italy
- ⁶³ Institute for Astronomy, University of Hawaii, 2680 Woodlawn Drive, Honolulu, HI 96822, USA
- ⁶⁴ Dipartimento di Fisica e Astronomia "Augusto Righi" - Alma Mater Studiorum Università di Bologna, Viale Berti Pichat 6/2, 40127 Bologna, Italy
- ⁶⁵ Instituto de Astrofísica de Canarias, Vía Láctea, 38205 La Laguna, Tenerife, Spain
- ⁶⁶ Institute for Astronomy, University of Edinburgh, Royal Observatory, Blackford Hill, Edinburgh EH9 3HJ, UK
- ⁶⁷ European Space Agency/ESRIN, Largo Galileo Galilei 1, 00044 Frascati, Roma, Italy
- ⁶⁸ Université Claude Bernard Lyon 1, CNRS/IN2P3, IP2I Lyon, UMR 5822, Villeurbanne, F-69100, France
- ⁶⁹ UCB Lyon 1, CNRS/IN2P3, IUF, IP2I Lyon, 4 rue Enrico Fermi, 69622 Villeurbanne, France
- ⁷⁰ Mullard Space Science Laboratory, University College London, Holmbury St Mary, Dorking, Surrey RH5 6NT, UK
- ⁷¹ Departamento de Física, Faculdade de Ciências, Universidade de Lisboa, Edifício C8, Campo Grande, PT1749-016 Lisboa, Portugal
- ⁷² Instituto de Astrofísica e Ciências do Espaço, Faculdade de Ciências, Universidade de Lisboa, Campo Grande, 1749-016 Lisboa, Portugal
- ⁷³ INAF-Istituto di Astrofisica e Planetologia Spaziali, via del Fosso del Cavaliere, 100, 00100 Roma, Italy
- ⁷⁴ Aix-Marseille Université, CNRS/IN2P3, CPPM, Marseille, France
- ⁷⁵ INFN-Bologna, Via Irnerio 46, 40126 Bologna, Italy
- ⁷⁶ School of Physics, HH Wills Physics Laboratory, University of Bristol, Tyndall Avenue, Bristol, BS8 1TL, UK
- ⁷⁷ FRACTAL S.L.N.E., calle Tulipán 2, Portal 13 1A, 28231, Las Rozas de Madrid, Spain
- ⁷⁸ Institute of Theoretical Astrophysics, University of Oslo, P.O. Box 1029 Blindern, 0315 Oslo, Norway
- ⁷⁹ Department of Physics, Lancaster University, Lancaster, LA1 4YB, UK
- ⁸⁰ Felix Hormuth Engineering, Goethestr. 17, 69181 Leimen, Germany
- ⁸¹ Technical University of Denmark, Elektrovej 327, 2800 Kgs. Lyngby, Denmark
- ⁸² Cosmic Dawn Center (DAWN), Denmark
- ⁸³ Max-Planck-Institut für Astronomie, Königstuhl 17, 69117 Heidelberg, Germany
- ⁸⁴ NASA Goddard Space Flight Center, Greenbelt, MD 20771, USA
- ⁸⁵ Department of Physics and Astronomy, University College London, Gower Street, London WC1E 6BT, UK
- ⁸⁶ Department of Physics and Helsinki Institute of Physics, Gustaf Hällströmin katu 2, 00014 University of Helsinki, Finland
- ⁸⁷ Université de Genève, Département de Physique Théorique and Centre for Astroparticle Physics, 24 quai Ernest-Ansermet, CH-1211 Genève 4, Switzerland
- ⁸⁸ Department of Physics, P.O. Box 64, 00014 University of Helsinki, Finland
- ⁸⁹ Helsinki Institute of Physics, Gustaf Hällströmin katu 2, University of Helsinki, Helsinki, Finland
- ⁹⁰ Centre de Calcul de l'IN2P3/CNRS, 21 avenue Pierre de Coubertin 69627 Villeurbanne Cedex, France
- ⁹¹ Laboratoire d'étude de l'Univers et des phénomènes eXtremes, Observatoire de Paris, Université PSL, Sorbonne Université, CNRS, 92190 Meudon, France
- ⁹² SKA Observatory, Jodrell Bank, Lower Withington, Macclesfield, Cheshire SK11 9FT, UK
- ⁹³ INFN-Sezione di Milano, Via Celoria 16, 20133 Milano, Italy
- ⁹⁴ University of Applied Sciences and Arts of Northwestern Switzerland, School of Computer Science, 5210 Windisch, Switzerland
- ⁹⁵ Universität Bonn, Argelander-Institut für Astronomie, Auf dem Hügel 71, 53121 Bonn, Germany
- ⁹⁶ Université Côte d'Azur, Observatoire de la Côte d'Azur, CNRS, Laboratoire Lagrange, Bd de l'Observatoire, CS 34229, 06304 Nice cedex 4, France
- ⁹⁷ Université Paris Cité, CNRS, Astroparticule et Cosmologie, 75013 Paris, France
- ⁹⁸ CNRS-UCB International Research Laboratory, Centre Pierre Binetruy, IRL2007, CPB-IN2P3, Berkeley, USA
- ⁹⁹ Institut d'Astrophysique de Paris, 98bis Boulevard Arago, 75014, Paris, France
- ¹⁰⁰ Aurora Technology for European Space Agency (ESA), Camino bajo del Castillo, s/n, Urbanización Villafranca del Castillo, Villanueva de la Cañada, 28692 Madrid, Spain
- ¹⁰¹ Institut de Física d'Altes Energies (IFAE), The Barcelona Institute of Science and Technology, Campus UAB, 08193 Bellaterra (Barcelona), Spain
- ¹⁰² DARK, Niels Bohr Institute, University of Copenhagen, Jagtvej 155, 2200 Copenhagen, Denmark
- ¹⁰³ Waterloo Centre for Astrophysics, University of Waterloo, Waterloo, Ontario N2L 3G1, Canada
- ¹⁰⁴ Department of Physics and Astronomy, University of Waterloo, Waterloo, Ontario N2L 3G1, Canada
- ¹⁰⁵ Perimeter Institute for Theoretical Physics, Waterloo, Ontario N2L 2Y5, Canada
- ¹⁰⁶ Centre National d'Etudes Spatiales – Centre spatial de Toulouse, 18 avenue Edouard Belin, 31401 Toulouse Cedex 9, France
- ¹⁰⁷ Institute of Space Science, Str. Atomistilor, nr. 409 Măgurele, Ilfov, 077125, Romania
- ¹⁰⁸ Consejo Superior de Investigaciones Científicas, Calle Serrano 117, 28006 Madrid, Spain
- ¹⁰⁹ Universidad de La Laguna, Departamento de Astrofísica, 38206 La Laguna, Tenerife, Spain
- ¹¹⁰ Dipartimento di Fisica e Astronomia "G. Galilei", Università di Padova, Via Marzolo 8, 35131 Padova, Italy
- ¹¹¹ INFN-Padova, Via Marzolo 8, 35131 Padova, Italy
- ¹¹² Institut für Theoretische Physik, University of Heidelberg, Philosophenweg 16, 69120 Heidelberg, Germany
- ¹¹³ Institut de Recherche en Astrophysique et Planétologie (IRAP), Université de Toulouse, CNRS, UPS, CNES, 14 Av. Edouard Belin, 31400 Toulouse, France
- ¹¹⁴ Université St Joseph; Faculty of Sciences, Beirut, Lebanon
- ¹¹⁵ Departamento de Física, FCFM, Universidad de Chile, Blanco Encalada 2008, Santiago, Chile
- ¹¹⁶ Universität Innsbruck, Institut für Astro- und Teilchenphysik, Technikerstr. 25/8, 6020 Innsbruck, Austria
- ¹¹⁷ Institut d'Estudis Espacials de Catalunya (IEEC), Edifici RDIT, Campus UPC, 08860 Castelldefels, Barcelona, Spain
- ¹¹⁸ Atlantis, University Science Park, Sede Bld 48940, Leioa-Bilbao, Spain
- ¹¹⁹ Institute of Space Sciences (ICE, CSIC), Campus UAB, Carrer de Can Magrans, s/n, 08193 Barcelona, Spain
- ¹²⁰ Department of Physics, Royal Holloway, University of London, TW20 0EX, UK
- ¹²¹ Instituto de Astrofísica e Ciências do Espaço, Faculdade de Ciências, Universidade de Lisboa, Tapada da Ajuda, 1349-018 Lisboa, Portugal
- ¹²² Cosmic Dawn Center (DAWN)

- ¹²³ Niels Bohr Institute, University of Copenhagen, Jagtvej 128, 2200 Copenhagen, Denmark
- ¹²⁴ Universidad Politécnica de Cartagena, Departamento de Electrónica y Tecnología de Computadoras, Plaza del Hospital 1, 30202 Cartagena, Spain
- ¹²⁵ Kapteyn Astronomical Institute, University of Groningen, PO Box 800, 9700 AV Groningen, The Netherlands
- ¹²⁶ Infrared Processing and Analysis Center, California Institute of Technology, Pasadena, CA 91125, USA
- ¹²⁷ Dipartimento di Fisica e Scienze della Terra, Università degli Studi di Ferrara, Via Giuseppe Saragat 1, 44122 Ferrara, Italy
- ¹²⁸ Istituto Nazionale di Fisica Nucleare, Sezione di Ferrara, Via Giuseppe Saragat 1, 44122 Ferrara, Italy
- ¹²⁹ INAF, Istituto di Radioastronomia, Via Piero Gobetti 101, 40129 Bologna, Italy
- ¹³⁰ Instituto de Astrofísica de Canarias (IAC); Departamento de Astrofísica, Universidad de La Laguna (ULL), 38200, La Laguna, Tenerife, Spain
- ¹³¹ Université PSL, Observatoire de Paris, Sorbonne Université, CNRS, LERMA, 75014, Paris, France
- ¹³² Université Paris-Cité, 5 Rue Thomas Mann, 75013, Paris, France
- ¹³³ INAF - Osservatorio Astronomico di Brera, via Emilio Bianchi 46, 23807 Merate, Italy
- ¹³⁴ INAF-Osservatorio Astronomico di Brera, Via Brera 28, 20122 Milano, Italy, and INFN-Sezione di Genova, Via Dodecaneso 33, 16146, Genova, Italy
- ¹³⁵ ICL, Junia, Université Catholique de Lille, LITL, 59000 Lille, France
- ¹³⁶ ICSC - Centro Nazionale di Ricerca in High Performance Computing, Big Data e Quantum Computing, Via Magnanelli 2, Bologna, Italy
- ¹³⁷ Instituto de Física Teórica UAM-CSIC, Campus de Cantoblanco, 28049 Madrid, Spain
- ¹³⁸ CERCA/ISO, Department of Physics, Case Western Reserve University, 10900 Euclid Avenue, Cleveland, OH 44106, USA
- ¹³⁹ Laboratoire Univers et Théorie, Observatoire de Paris, Université PSL, Université Paris Cité, CNRS, 92190 Meudon, France
- ¹⁴⁰ Departamento de Física Fundamental, Universidad de Salamanca, Plaza de la Merced s/n. 37008 Salamanca, Spain
- ¹⁴¹ Université de Strasbourg, CNRS, Observatoire astronomique de Strasbourg, UMR 7550, 67000 Strasbourg, France
- ¹⁴² Center for Data-Driven Discovery, Kavli IPMU (WPI), UTIAS, The University of Tokyo, Kashiwa, Chiba 277-8583, Japan
- ¹⁴³ California Institute of Technology, 1200 E California Blvd, Pasadena, CA 91125, USA
- ¹⁴⁴ Department of Physics & Astronomy, University of California Irvine, Irvine CA 92697, USA
- ¹⁴⁵ Department of Mathematics and Physics E. De Giorgi, University of Salento, Via per Arnesano, CP-193, 73100, Lecce, Italy
- ¹⁴⁶ INFN, Sezione di Lecce, Via per Arnesano, CP-193, 73100, Lecce, Italy
- ¹⁴⁷ INAF-Sezione di Lecce, c/o Dipartimento Matematica e Fisica, Via per Arnesano, 73100, Lecce, Italy
- ¹⁴⁸ Instituto de Física de Cantabria, Edificio Juan Jordá, Avenida de los Castros, 39005 Santander, Spain
- ¹⁴⁹ CEA Saclay, DFR/IRFU, Service d'Astrophysique, Bat. 709, 91191 Gif-sur-Yvette, France
- ¹⁵⁰ Department of Computer Science, Aalto University, PO Box 15400, Espoo, FI-00 076, Finland
- ¹⁵¹ Instituto de Astrofísica de Canarias, c/ Via Lactea s/n, La Laguna 38200, Spain. Departamento de Astrofísica de la Universidad de La Laguna, Avda. Francisco Sanchez, La Laguna, 38200, Spain
- ¹⁵² Ruhr University Bochum, Faculty of Physics and Astronomy, Astronomical Institute (AIRUB), German Centre for Cosmological Lensing (GCCL), 44780 Bochum, Germany
- ¹⁵³ Astrophysics Research Centre, University of KwaZulu-Natal, Westville Campus, Durban 4041, South Africa
- ¹⁵⁴ School of Mathematics, Statistics & Computer Science, University of KwaZulu-Natal, Westville Campus, Durban 4041, South Africa
- ¹⁵⁵ Department of Physics and Astronomy, Vesilinnantie 5, 20014 University of Turku, Finland
- ¹⁵⁶ Serco for European Space Agency (ESA), Camino bajo del Castillo, s/n, Urbanizacion Villafranca del Castillo, Villanueva de la Cañada, 28692 Madrid, Spain
- ¹⁵⁷ ARC Centre of Excellence for Dark Matter Particle Physics, Melbourne, Australia
- ¹⁵⁸ Centre for Astrophysics & Supercomputing, Swinburne University of Technology, Hawthorn, Victoria 3122, Australia
- ¹⁵⁹ Department of Physics and Astronomy, University of the Western Cape, Bellville, Cape Town, 7535, South Africa
- ¹⁶⁰ DAMTP, Centre for Mathematical Sciences, Wilberforce Road, Cambridge CB3 0WA, UK
- ¹⁶¹ Kavli Institute for Cosmology Cambridge, Madingley Road, Cambridge, CB3 0HA, UK
- ¹⁶² Department of Astrophysics, University of Zurich, Winterthurerstrasse 190, 8057 Zurich, Switzerland
- ¹⁶³ IRFU, CEA, Université Paris-Saclay 91191 Gif-sur-Yvette Cedex, France
- ¹⁶⁴ Oskar Klein Centre for Cosmoparticle Physics, Department of Physics, Stockholm University, Stockholm, SE-106 91, Sweden
- ¹⁶⁵ Astrophysics Group, Blackett Laboratory, Imperial College London, London SW7 2AZ, UK
- ¹⁶⁶ Univ. Grenoble Alpes, CNRS, Grenoble INP, LPSC-IN2P3, 53, Avenue des Martyrs, 38000, Grenoble, France
- ¹⁶⁷ INAF-Osservatorio Astrofisico di Arcetri, Largo E. Fermi 5, 50125, Firenze, Italy
- ¹⁶⁸ Dipartimento di Fisica, Sapienza Università di Roma, Piazzale Aldo Moro 2, 00185 Roma, Italy
- ¹⁶⁹ Centro de Astrofísica da Universidade do Porto, Rua das Estrelas, 4150-762 Porto, Portugal
- ¹⁷⁰ Dipartimento di Fisica, Università di Roma Tor Vergata, Via della Ricerca Scientifica 1, Roma, Italy
- ¹⁷¹ INFN, Sezione di Roma 2, Via della Ricerca Scientifica 1, Roma, Italy
- ¹⁷² HE Space for European Space Agency (ESA), Camino bajo del Castillo, s/n, Urbanizacion Villafranca del Castillo, Villanueva de la Cañada, 28692 Madrid, Spain
- ¹⁷³ Dipartimento di Fisica - Sezione di Astronomia, Università di Trieste, Via Tiepolo 11, 34131 Trieste, Italy
- ¹⁷⁴ Department of Astrophysical Sciences, Peyton Hall, Princeton University, Princeton, NJ 08544, USA
- ¹⁷⁵ Theoretical astrophysics, Department of Physics and Astronomy, Uppsala University, Box 515, 751 20 Uppsala, Sweden
- ¹⁷⁶ Minnesota Institute for Astrophysics, University of Minnesota, 116 Church St SE, Minneapolis, MN 55455, USA
- ¹⁷⁷ Mathematical Institute, University of Leiden, Einsteinweg 55, 2333 CA Leiden, The Netherlands
- ¹⁷⁸ Institute of Astronomy, University of Cambridge, Madingley Road, Cambridge CB3 0HA, UK
- ¹⁷⁹ Space physics and astronomy research unit, University of Oulu, Pentti Kaiteran katu 1, FI-90014 Oulu, Finland
- ¹⁸⁰ Department of Physics and Astronomy, Lehman College of the CUNY, Bronx, NY 10468, USA
- ¹⁸¹ American Museum of Natural History, Department of Astrophysics, New York, NY 10024, USA
- ¹⁸² Center for Computational Astrophysics, Flatiron Institute, 162 5th Avenue, 10010, New York, NY, USA
- ¹⁸³ Department of Physics and Astronomy, University of British Columbia, Vancouver, BC V6T 1Z1, Canada

Appendix A: Other DSPL lens candidates

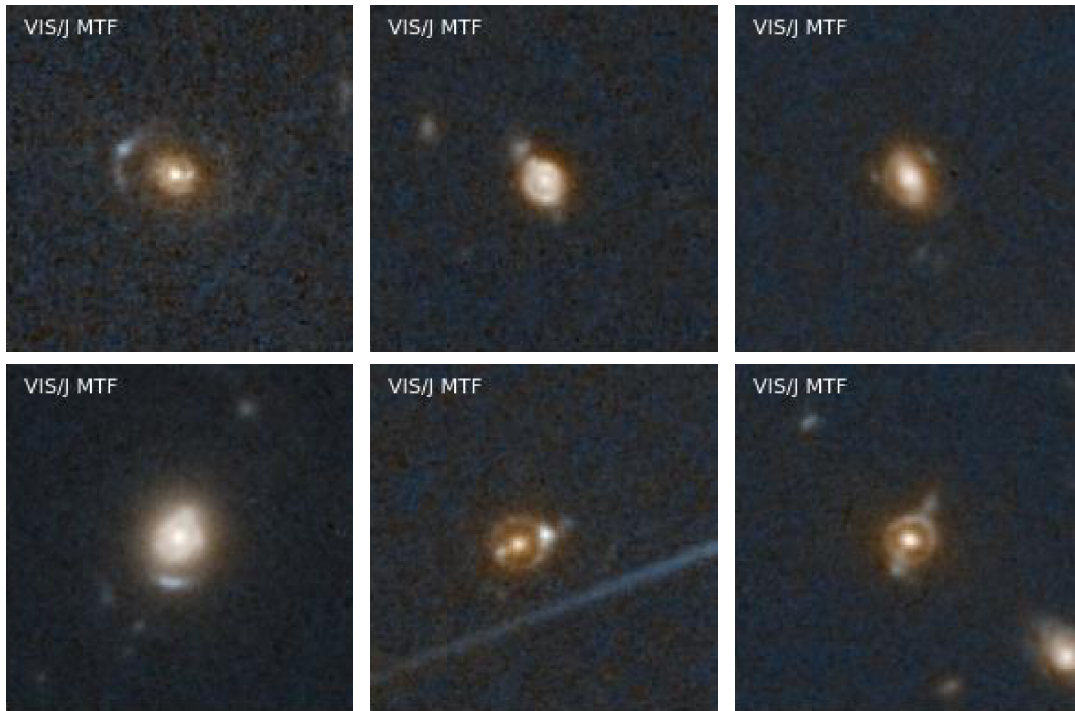


Fig. A.1. Low probability DSPL candidates selected among the top 1000 ranked galaxies in Galaxy Judges.

Due to the large survey area and high-resolution images provided by *Euclid*, rarer single-plane lensing configurations, and false positives can be discovered which could be misidentified as possible DSPL systems. Figure A.1 shows a sample of lens candidates in Q1 which might be DSPLs but we can not classify them with confidence due to their small Einstein radii. Figure A.2 shows a sample of images that could be confused for DSPLs but we believe are most likely contaminants. Here we outline several candidate configurations that create images that are similar to DSPLs:

- Double cusp configuration: When a source is positioned near a cusp of the tangential caustic, three closely spaced lensed images appear in the lens plane, while a fourth, more isolated and typically less magnified image, forms at a closer distance. If two sources within the same source plane are located near two opposing cusps of the diamond-shaped caustic, the resulting lensing configuration can produce a ring-like structure near the lens, along with two smaller arcs inside the ring. This configuration may resemble a DSPL system and could be mistakenly identified as such.
- Spiral galaxy and lens: In strong-lensing systems where the deflector is a spiral galaxy, features like spiral arms or star-forming rings can sometimes be misidentified as secondary rings at different (smaller or larger) radii. This is because star-forming regions often exhibit a distinct blue colour, similar to that of background lensed sources. Such cases are not common, as face-on spiral galaxies typically have low projected surface mass density, resulting in a small lensing cross-section. However, at least two possible cases were found in our sample although they may not even be lenses. This type of lens has its unique value but it's beyond the scope of this paper.



Fig. A.2. Candidate DSPL imposters selected among the top 1000 ranked galaxies in Galaxy Judges.

- Spiral galaxy with multiple arms: As described above, spiral arms can resemble lensed arcs, making certain spiral galaxies appear similar to DSPL systems. This is particularly true when the central bulge of the galaxy is large enough to mimic the appearance of an elliptical galaxy. However, such systems can typically be easily ruled out through lens modelling.
- Elliptical lens with complex shells: In addition to spiral arms, the shell structures of elliptical galaxies can also resemble lensed arcs. These features become more apparent after subtracting the lens light in preliminary lens modelling (Euclid Collaboration: Walmsley et al. 2025). However, such structures are often noisy, as they are typically buried beneath the bright lens light, making them more challenging to identify without careful analysis.
- Lens system with nearby galaxies: galaxies located close in projection to a lens but outside the multiply imaged region can mimic an image from a doubly lensed system. An expert might incorrectly guess that there is an undetected counter-image of this galaxy close to the centre of the primary lens.

The scenarios described above represent the most common cases where DSPL systems can be misidentified. Conversely, a genuine DSPL system can also be misclassified as one of these cases. To make a definitive determination either lens modelling of higher angular resolution images or spectroscopic redshifts for each component, are required.